Phenomenological formulation of hybrid transverse magneto-thermoelectric conversion in artificially tilted multilayers

Fuyuki Ando,[1,*] Yebin Lee,[1] Takamasa Hirai,[1] and Ken-ichi Uchida[1,2]

[1]*National Institute for Materials Science, 1-2-1 Sengen, Tsukuba, Ibaraki 305-0047, Japan*
[2]*Department of Advanced Materials Science, Graduate School of Frontier Sciences, The University of Tokyo, 5-1-5 Kashiwanoha, Kashiwa, Chiba 277-8561, Japan*

Hybridizing multiple transverse thermoelectric effects in a single material synergistically enhances the dimensionless figure of merit for transverse thermoelectric conversion owing to the square-law characteristics of the superimposed transverse thermopowers. Here, we phenomenologically formulate the appearance of transverse magneto-thermoelectric phenomena, i.e., the anomalous Nernst effect and Seebeck-driven anomalous Hall effect, in artificially tilted multilayers consisting of magnetic and thermoelectric materials, where the off-diagonal Seebeck effect originally exists due to the anisotropic composite structure. Because the contributions of the anomalous Nernst, Seebeck-driven anomalous Hall, and off-diagonal Seebeck effects to transverse thermopower have different artificial structure dependences with each other, the total thermoelectric performance maximizes by optimizing the structure to balance these effects. We confirm the appearance of these thermoelectric effects by performing a finite element analysis of transverse thermoelectric fields in artificially tilted multilayers consisting of ferromagnetic Co_2MnGa Heusler alloy and thermoelectric semiconductor Bi_2Te_3. This work will be a guideline to design the optimum structural parameters for superior transverse thermoelectric performance through the hybridization of spin- and magnetism-related thermoelectric phenomena in artificially tilted multilayers.

I. INTRODUCTION

Transverse thermoelectric effects, where charge and heat currents are converted in the orthogonal directions in solids, has recently attracted attention in the fields of solid-state physics, materials science, and thermal management applications [1–4]. This unique conversion geometry enables a simplification of thermoelectric device architecture only using a single material and attaching electrodes at the ends, which is a practical advantage against the conventional Seebeck-effect-based devices consisting of many pairs of *p*- and *n*-type thermoelectric elements [5–8]. Owing to this junctionless structure, transverse thermoelectric devices have potential to exhibit ideal thermoelectric performance expected from the constituent material.

Multiple principles of the transverse thermoelectric conversion have been investigated so far. The most representative ones are the ordinary Nernst effect in nonmagnetic conductors [1] and anomalous Nernst effect (ANE) in magnetic materials. Especially, associated with the development of spin caloritronics [3,9–11] and topological materials science [12–14], both theoretical and experimental studies on ANE have rapidly progressed realizing superior transverse thermoelectric performance due to non-trivial band topology [15–25] or extrinsic charge-spin scattering mechanisms [26–28]. Recently, Zhou et al. demonstrated a unique way to boost the transverse thermopower by a hybrid action of the Seebeck and anomalous Hall effects in thermoelectric semiconductor/ferromagnetic metal heterostructures, which is called the Seebeck-driven magneto-thermoelectric conversion or Seebeck-driven anomalous Hall effect (SAHE) (note that we adopt the latter terminology in this paper) [29–32]. Meanwhile, as the transverse thermoelectric effect unrelated to magnetism, the off-diagonal Seebeck effect (ODSE) has been intensively studied for wide variety of materials including goniopolar materials [33–37], $p \times n$-type superlattices [38,39], and artificially tilted multilayers [40–45]. These ODSE materials tend to exhibit higher transverse thermoelectric performance than those by spin- or magnetism-related principles.

Hybridization of the multiple transverse thermoelectric effects in a single material paves a new way to realize an unprecedentedly high thermoelectric performance [46–48]. Uchida et al. first demonstrated the hybrid transverse magneto-thermoelectric conversion in $Bi_{88}Sb_{12}/Bi_{0.2}Sb_{1.8}Te_3$-based artificially tilted multilayers, where the magneto-Seebeck and ordinary Nernst effects mainly in the $Bi_{88}Sb_{12}$ layers are superimposed on ODSE by the application of an external magnetic field. As a result, the total transverse thermoelectric cooling performance was largely modulated from -10% to +15% [46]. ANE was also superimposed by embedding magnetic layers in artificially tilted multilayers [47], which was achieved

*Contact author: ANDO.Fuyuki@nims.go.jp

even without an external magnetic field by the use of permanent magnet materials [48]. The figure of merit $z_{xy}T$ for this hybrid transverse thermoelectric conversion is expressed as

$$z_{xy}T = \frac{{S_{xy}}^2}{\rho_{xx}\kappa_{yy}}T = \frac{\left[S_{\mathrm{ODSE}} + S_{xy}(M \text{ or } H)\right]^2}{\rho_{xx}\kappa_{yy}}T$$
$$= \frac{{S_{\mathrm{ODSE}}}^2 + S_{xy}(M \text{ or } H)^2 + 2S_{\mathrm{ODSE}} \cdot S_{xy}(M \text{ or } H)}{\rho_{xx}\kappa_{yy}}T. \tag{1}$$

Here, the total transverse thermopower S_{xy} is the sum of the transverse thermopower due to ODSE (S_{ODSE}) and that dependent on the magnetization M or magnetic field H [$S_{xy}(M$ or $H)$]. ρ_{xx} is the electrical resistivity along the direction of a charge current, κ_{yy} is the thermal conductivity along the direction of a heat current, and T is the absolute temperature. Because $z_{xy}T$ is proportional to the square of S_{xy}, $S_{xy}(M$ or $H)$ produces the $2S_{\mathrm{ODSE}}{\cdot}S_{xy}(M$ or $H)$ term in addition to $S_{xy}(M$ or $H)^2$, which offers the greater improvement of $z_{xy}T$ than that solely by $S_{xy}(M$ or $H)^2$.

However, there remains a problem that the $S_{xy}(M$ or $H)$ value is unclear in artificially tilted multilayers, which differs from the transverse magneto-thermopower of magnetic layers, such as the anomalous Nernst coefficient S_{ANE}, due to the inhomogeneous temperature distribution and electrical shunting with the adjacent layers [47]. Furthermore, $S_{xy}(M$ or $H)$ has a structural parameter dependence different from that of S_{ODSE}. Thus, we need a guideline for the optimum composite structure to balance S_{ODSE} and $S_{xy}(M$ or $H)$ and maximize transverse thermoelectric performance.

In this study, we phenomenologically developed the formulation of the hybrid transverse magneto-thermopower S_{xy} [$=S_{\mathrm{ODSE}}+S_{xy}(M$ or $H)$] for artificially tilted multilayers consisting of magnetic and thermoelectric materials as shown in Fig. 1. Electric fields **E** induced by ANE and SAHE in magnetic layers are formulated for multilayers with a tilt angle $\theta = 0°$. The coordinate rotation in x-y plane yields the ODSE-induced **E** and resultant S_{xy}. To confirm the appearance of these thermoelectric effects, we perform a thermoelectric coupling analysis using a finite element method (FEM) for the artificially tilted multilayers consisting of a ferromagnetic Co_2MnGa Heusler alloy and thermoelectric Bi_2Te_3 compound. The analysis shows that the $S_{xy}(M$ or $H)$ term has a unique structural parameter dependence which modifies the optimum composite structure and a sizable impact on S_{xy} and $z_{xy}T$.

II. METHODS

Figure 1 shows a multilayer system for the tensor calculation of S_{xy}. Magnetic and thermoelectric

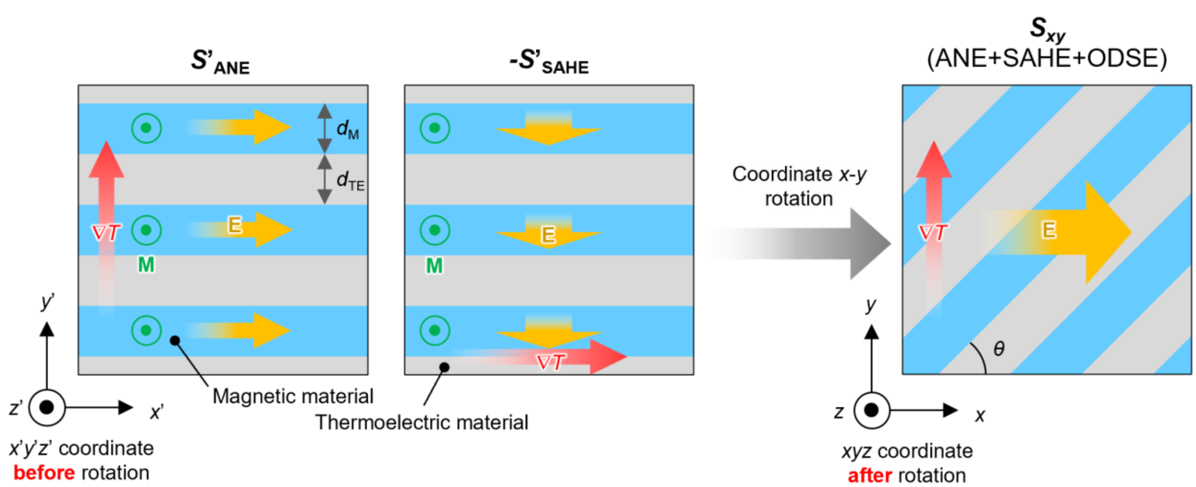

FIG 1. Schematic of transverse magneto-thermoelectric conversion in artificially tilted multilayers consisting of magnetic and thermoelectric materials. S'_{ANE} and S'_{SAHE} are defined as $\mathbf{E}'_x$ and $\mathbf{E}'_y$ divided by $\nabla'_y T$ and $\nabla'_x T$, respectively. S'_{ANE} refers to the transverse thermopower induced by ANE in the magnetic layers with **M** along the z'-direction, whereas S'_{SAHE} by ANE and SAHE through the contribution from the neighboring thermoelectric layers. The tensor calculation of S_{xy} by all the ANE, SAHE, and ODSE contributions in the artificially tilted multilayers is performed by rotating the coordinate with θ from the $x'y'z'$ to xyz Cartesian coordinate.

*Contact author: ANDO.Fuyuki@nims.go.jp

materials are alternately stacked in the y'-direction of $x'y'z'$ Cartesian coordinate system. The thickness ratio of the magnetic layers relative to the total thickness $t = d_M/(d_M+d_{TE})$ is fixed, where d_M and d_{TE} are the thicknesses of the magnetic and thermoelectric layers, respectively. When **M** is oriented along the z'-direction and a temperature gradient ∇T is applied in the x'-y' plane, **E** is induced in the cross-product ($\nabla T\times\mathbf{M}$) direction by ANE and SAHE. S'_{ANE} and S'_{SAHE} are respectively defined as the generation of $\mathbf{E}'_x$ and $\mathbf{E}'_y$ induced by $\nabla'_y T$ and $\nabla'_x T$.

Table I shows thermoelectric, electrical, and thermal transport phenomena for constituent materials which are dealt in or applicable to our framework. In this work, we simplify the model as much as possible focusing on the essential phenomena to discuss the importance of the hybrid strategy. For the diagonal terms in thermoelectric tensor S_{ij}, we assume an isotropic Seebeck coefficient as $S_{xx} = S_{yy}$ (= S), which can be extended to the isotropic magneto-Seebeck effect. Note that, however, the anisotropic (magneto-)Seebeck effect is out of our framework. For the off-diagonal terms, we account ANE induced by **M** as $S_{xy} = -S_{yx}$ (= S_{ANE}) at $m_z = +1$, excluding the ordinary Nernst effect induced by **H** and S_{ODSE} ($S_{xy} = S_{yx}$) of constituents induced by the microscopic structural symmetry breaking [4]. Also, we assume isotropic longitudinal electrical and thermal conductivities as $\sigma_{xx} = \sigma_{yy}$ (= σ) and $\kappa_{xx} = \kappa_{yy}$ (= κ), which include magneto-resistance and magneto-thermal resistance effect as far as they are isotropic. For the off-diagonal terms, only AHE induced by **M** is accountable, whereas the ordinary and symmetric Hall effects [49], ordinary and anomalous Righi-Leduc effects [50,51], and off-diagonal thermal conduction by structural symmetry breaking [52] are not. Please note that the following discussion is valid when the effects in the "Phenomena" column in Table I are accounted. We list the main physical quantities used in this study in Table II.

First, we formulate S'_{ANE} in a multilayer system. The effective temperature gradient applied to the magnetic layers in the y'-direction is described as $t\kappa^{TE}\nabla T/[t\kappa^{TE}+(1-t)\kappa^{M}]$ with κ^{M} and κ^{TE} respectively being thermal conductivities of the magnetic and thermoelectric materials. The generated $\mathbf{E}'_x$ for the magnetic layers with $S_{\mathrm{ANE}}^{\mathrm{M}}$ is reduced by the factor $t\sigma^{M}/[t\sigma^{M}+(1-t)\sigma^{TE}]$ due to electrical shunting with the neighboring thermoelectric layers, where σ^{M} and σ^{TE} are electrical conductivities of the magnetic and thermoelectric materials, respectively. Consequently, the transverse magneto-thermopower S'_{ANE} normalized by $\nabla'_y T$ is expressed as

$$S'_{\mathrm{ANE}}(m_z) = \frac{t\kappa^{\mathrm{TE}}}{t\kappa^{\mathrm{TE}}+(1-t)\kappa^{\mathrm{M}}}\frac{t\sigma^{\mathrm{M}}}{t\sigma^{\mathrm{M}}+(1-t)\sigma^{\mathrm{TE}}}S_{\mathrm{ANE}}^{\mathrm{M}}\cdot m_z. \tag{2}$$

Here, m_z is the z' component of the unit magnetization vector ($-1 \le m_z \le +1$).

Next, we formulate S'_{SAHE} as well as S'_{ANE}. When $\nabla'_x T$ is applied, a charge current is induced by the difference of the Seebeck coefficients between the magnetic and thermoelectric materials ($S^{\mathrm{TE}}-S^{\mathrm{M}}$). The shunting charge current in magnetic layers is in

TABLE I. Thermoelectric, electrical, and thermal transport phenomena for constituents applicable to this study.

	Symmetry	Phenomena	Not applicable
S_{ii}	$S_{xx} = S_{yy}$ (= S)	Magneto-Seebeck effect	Anisotropic magneto-Seebeck effect
S_{ij}	$S_{xy} = -S_{yx}$ (= S_{ANE})	Anomalous Nernst effect	Ordinary Nernst effect Off-diagonal Seebeck effect
σ_{ii} (σ)	$\sigma_{xx} = \sigma_{yy}$ (= σ)	Magneto-resistance	Anisotropic magneto-resistance
σ_{ij}	$\sigma_{xy} = -\sigma_{yx}$ (= σ_{AHE})	Anomalous Hall effect	Ordinary and symmetric Hall effect
κ_{ii}	$\kappa_{xx} = \kappa_{yy}$ (= κ)	Magneto-thermal resistance	Anisotropic magneto-thermal resistance
κ_{ij}	$\kappa_{xy} = -\kappa_{yx}$ (= 0)	/	Ordinary and anomalous Righi-Leduc effects Off-diagonal thermal conduction

*Contact author: ANDO.Fuyuki@nims.go.jp

TABLE II. Summary of the main physical quantities.

Structural parameter	
θ [°]	Tilt angle
t [a.u.]	Thickness ratio
Constituent material	
S [V/K]	Seebeck coefficient
σ [S/m]	Electrical conductivity
κ [W/m·K]	Thermal conductivity
S_{ANE} [V/K]	Anomalous Nernst coefficient
$\tan\theta_{\mathrm{AHE}}$ [a.u.]	Anomalous Hall angle ($= -\sigma_{\mathrm{AHE}}/\sigma$)
m_z [a.u.]	Unit magnetization vector in $z(z')$-direction
Multilayer system ($\theta = 0°$, $x'y'z'$ coordinate)	
S'_{xx} [V/K]	Longitudinal thermopower $\mathbf{E}'_x$ induced by $\nabla'_x T$
S'_{yy} [V/K]	Longitudinal thermopower $\mathbf{E}'_y$ induced by $\nabla'_y T$
S'_{ANE} [V/K]	Transverse thermopower $\mathbf{E}'_x$ induced by $\nabla'_y T$
S'_{SAHE} [V/K]	Transverse thermopower $\mathbf{E}'_y$ induced by $\nabla'_x T$
Artificially tilted multilayer system ($\theta \neq 0°$, xyz coordinate)	
S_{ODSE} [V/K]	Transverse thermopower by ODSE
S_{xy} [V/K]	Hybrid transverse thermopower by ODSE, ANE, and SAHE
ρ_{xx} [Ω·m]	Electrical resistivity
κ_{yy} [W/m·K]	Thermal conductivity
$z_{xy}T$ [a.u.]	Transverse thermoelectric figure of merit

turn converted into transverse $\mathbf{E}'_y$ by AHE [31]. Then, $S^{\mathrm{M}}_{\mathrm{ANE}}$ is modified into

$$S^{\mathrm{M}}_{\mathrm{ANE}} - \frac{(1-t)(S^{\mathrm{TE}} - S^{\mathrm{M}})\sigma^{\mathrm{TE}}\tan\theta^{\mathrm{M}}_{\mathrm{AHE}}}{t\sigma^{\mathrm{M}} + (1-t)\sigma^{\mathrm{TE}}}, \quad (3)$$

Because $\mathbf{E}'_y$ appears only in the magnetic layers as shown in Fig. 1, S'_{SAHE} for the whole multilayer system is expressed as

$$S'_{\mathrm{SAHE}}(m_z) = -t\left[S^{\mathrm{M}}_{\mathrm{ANE}} - \frac{(1-t)(S^{\mathrm{TE}} - S^{\mathrm{M}})\sigma^{\mathrm{TE}}\tan\theta^{\mathrm{M}}_{\mathrm{AHE}}}{t\sigma^{\mathrm{M}} + (1-t)\sigma^{\mathrm{TE}}}\right]\cdot m_z. \quad (4)$$

Utilizing S'_{ANE} and S'_{SAHE} in a multilayer system, we obtain S_{xy} for an artificially tilted multilayer system with a finite θ value. The thermoelectric tensor in the $x'y'z'$ coordinate is given by

$$S'_{ij} = \begin{pmatrix} S'_{xx} & S'_{\mathrm{ANE}} & 0 \\ S'_{\mathrm{SAHE}} & S'_{yy} & 0 \\ 0 & 0 & S'_{zz} \end{pmatrix}. \quad (5)$$

Here, S'_{xx} and S'_{yy} are described as follows:

$$S'_{xx} = \frac{t\sigma^{\mathrm{M}}S^{\mathrm{M}} + (1-t)\sigma^{\mathrm{TE}}S^{\mathrm{TE}}}{t\sigma^{\mathrm{M}} + (1-t)\sigma^{\mathrm{TE}}}, \quad (6)$$

$$S'_{yy} = \frac{t\kappa^{\mathrm{TE}}S^{\mathrm{M}} + (1-t)\kappa^{\mathrm{M}}S^{\mathrm{TE}}}{t\kappa^{\mathrm{TE}} + (1-t)\kappa^{\mathrm{M}}}. \quad (7)$$

To transform Eq. (5) for the case of an artificially tilted multilayer, we introduce a rotation of θ around the z'-axis. This modifies the original $x'y'z'$ Cartesian coordinate with $x = x'\cos\theta + y'\sin\theta$ and $y = -x'\sin\theta + y'\cos\theta$ by the Jacobian matrix of the coordinate transformation:

$$J = \begin{pmatrix} \cos\theta & \sin\theta & 0 \\ -\sin\theta & \cos\theta & 0 \\ 0 & 0 & 1 \end{pmatrix}. \quad (8)$$

As a result, S_{xy} component in the thermoelectric tensor S_{ij} for artificially tilted multilayers is expressed as

$$S_{xy} = (S'_{xx} - S'_{yy})\sin\theta\cos\theta + S'_{\mathrm{ANE}}(m_z)\cos^2\theta - S'_{\mathrm{SAHE}}(m_z)\sin^2\theta. \quad (9)$$

*Contact author: ANDO.Fuyuki@nims.go.jp

The first term $(S'_{xx}-S'_{yy})\sin\theta\cos\theta$ corresponds to S_{ODSE} as the Goldsmid proposed [41] and the second term $S'_{ANE}(m_z)\cos^2\theta-S'_{SAHE}(m_z)\sin^2\theta$ to the magnetization-dependent term $S_{xy}(M$ or $H)$. For a fixed t value, the derivative of S_{xy} by θ is expressed as

$$\frac{dS_{xy}}{d\theta} = (S'_{xx} - S'_{yy})\cos 2\theta \\ -[S'_{\mathrm{ANE}}(m_z) + S'_{\mathrm{SAHE}}(m_z)]\sin 2\theta. \tag{10}$$

Then, the stationary θ value at $dS_{xy}/d\theta = 0$ satisfies

$$\tan 2\theta = \frac{S'_{xx} - S'_{yy}}{S'_{\mathrm{ANE}}(m_z) + S'_{\mathrm{SAHE}}(m_z)}, \tag{11}$$

which provides the appropriate branch to identify the maximum S_{xy} value. Furthermore, according to the following equation,

$$\left.\frac{dS_{xy}}{d\theta}\right|_{\theta=45^\circ} = -[S'_{\mathrm{ANE}}(m_z) + S'_{\mathrm{SAHE}}(m_z)], \tag{12}$$

one can find the optimum θ value to maximize S_{xy} shifts above (below) 45° when $S'_{ANE}(m_z)+S'_{SAHE}(m_z)$ is negative (positive).

Then, let us introduce physical criteria to enhance and constructively hybridize ODSE, ANE, and SAHE. For the first term $[S_{ODSE} = (S'_{xx}-S'_{yy})\sin\theta\cos\theta]$, $S'_{xx}-S'_{yy}$ is obtained by the transformation of Eqs. (6)–(7) as follows,

$$S'_{xx} - S'_{yy} \\ = \left[\frac{t\sigma^{\mathrm{M}}}{t\sigma^{\mathrm{M}} + (1-t)\sigma^{\mathrm{TE}}} - \frac{t\kappa^{\mathrm{TE}}}{t\kappa^{\mathrm{TE}} + (1-t)\kappa^{\mathrm{M}}}\right] S^{\mathrm{M}} \\ + \left[\frac{(1-t)\sigma^{\mathrm{TE}}}{t\sigma^{\mathrm{M}} + (1-t)\sigma^{\mathrm{TE}}} - \frac{(1-t)\kappa^{\mathrm{M}}}{t\kappa^{\mathrm{TE}} + (1-t)\kappa^{\mathrm{M}}}\right] S^{\mathrm{TE}}. \tag{13}$$

When inequal relationships of $\sigma^M > \sigma^{TE}$ and $\kappa^M > \kappa^{TE}$ are assumed, the opposite sign of S^M and S^{TE} is necessary to constructively superpose the first and second terms in Eq. (13) with the same sign. Meanwhile, one can achieve a constructive hybridization of ANE and SAHE for the higher value of second term $[S'_{ANE}(m_z)\cos^2\theta-S'_{SAHE}(m_z)\sin^2\theta]$ by satisfying the following sign criterion as,

$$S^{\mathrm{M}}_{\mathrm{ANE}} \cdot (S^{\mathrm{TE}} - S^{\mathrm{M}}) \cdot \tan\theta^{\mathrm{M}}_{\mathrm{AHE}} < 0. \tag{14}$$

Because the sign of second term depends on that of m_z, one can constructively superpose the first (ODSE) and second (ANE and SAHE) terms in Eq. (9) by optimizing the magnetization direction. Thus, to obtain the higher S_{xy}, one needs to select the constituent materials simultaneously taking Eq. (13) and the inequality (14) into account.

To discuss the quantitative impact of the superposition of the second (ANE and SAHE) term on the transverse thermoelectric performance, we analytically calculate S_{xy} and $z_{xy}T$ for the artificially tilted multilayers based on the ferromagnetic Co_2MnGa Heusler alloy with large S_{ANE} and $\tan\theta_{AHE}$ [18,19] and thermoelectric Bi_2Te_3 compound with larger S than Co_2MnGa. Table III summarizes the transport properties for Co_2MnGa and Bi_2Te_3 [31,47,53]. This material combination satisfies the sign criterion (14), ensuring the constructive hybridization of ANE and SAHE.

We also performed an FEM simulation by COMSOL Multiphysics software to confirm the appearance of ANE and SAHE in artificially tilted multilayers. 2-dimensional Co_2MnGa/Bi_2Te_3-based artificially tilted multilayers with an area of 10.0 × 8.0 mm^2 and θ of 0, 15, 30, 45, 60, 75, and 90° were constructed. The thicknesses of the Co_2MnGa and Bi_2Te_3 layers are respectively set to be 1.0 mm and 0.7 mm, where t is 0.59, which is comparable to the experimentally demonstrated value in ref. [47]. Temperatures on the top and bottom sides are set to be 303.15 K and 293.15 K, respectively. The interfacial electrical and thermal resistance between Co_2MnGa and Bi_2Te_3 layers are set to be zero, limiting our framework into an ideal SAHE-enhanced regime.

TABLE III. Transport properties for Co_2MnGa and Bi_2Te_3 [31,46].

	S^M, S^{TE} [×10^{-6} V/K]	σ^M, σ^{TE} [×10^5 S/m]	κ^M, κ^{TE} [W/m·K]	S^M_{ANE} [×10^{-6} V/K]	$\tan\theta^M_{AHE}$ [a.u.]
Co_2MnGa	–32.1	7.99	18.7	6.9	0.089
Bi_2Te_3	–110.3	1.83	1.5	n.a.	n.a.

*Contact author: ANDO.Fuyuki@nims.go.jp

III. RESULTS

A. Tensor calculation

Figure 2(a)–(b) shows the tensor calculation results of $S'_{\mathrm{ANE}}(m_z = +1)\cos^2\theta$ and $-S'_{\mathrm{SAHE}}(m_z = +1)\sin^2\theta$ for the Co_2MnGa/Bi_2Te_3-based artificially tilted multilayer. $S'_{\mathrm{ANE}}(m_z = +1)\cos^2\theta$ increases with the increase of t and decrease of θ due to the $\cos^2\theta$ contribution and reaches 6.9×10^{-6} V/K at $\theta = 0°$ and $t = 1.0$, that is, $S^{\mathrm{M}}_{\mathrm{ANE}}$ of plain Co_2MnGa. Meanwhile, $-S'_{\mathrm{SAHE}}(m_z = +1)\sin^2\theta$ increases with increasing both t and θ due to the $\sin^2\theta$ contribution, which interestingly exhibits relatively larger values in the wide range of t and θ than $S'_{\mathrm{ANE}}(m_z = +1)\cos^2\theta$. This characteristic is attributed not only to the absence of inhomogeneous temperature distribution and electrical shunting but also to the constructive hybridization of ANE and SAHE according to the inequality (14).

Figure 2(c) shows the calculated S_{ODSE} for the Co_2MnGa/Bi_2Te_3-based artificially tilted multilayer. Regardless of the m_z value, the finite S_{ODSE} is induced due to the anisotropy of the Seebeck coefficient (S'_{xx}–S'_{yy}) and maximized at $\theta = 45°$ because of the $\sin\theta\cos\theta$ contribution.

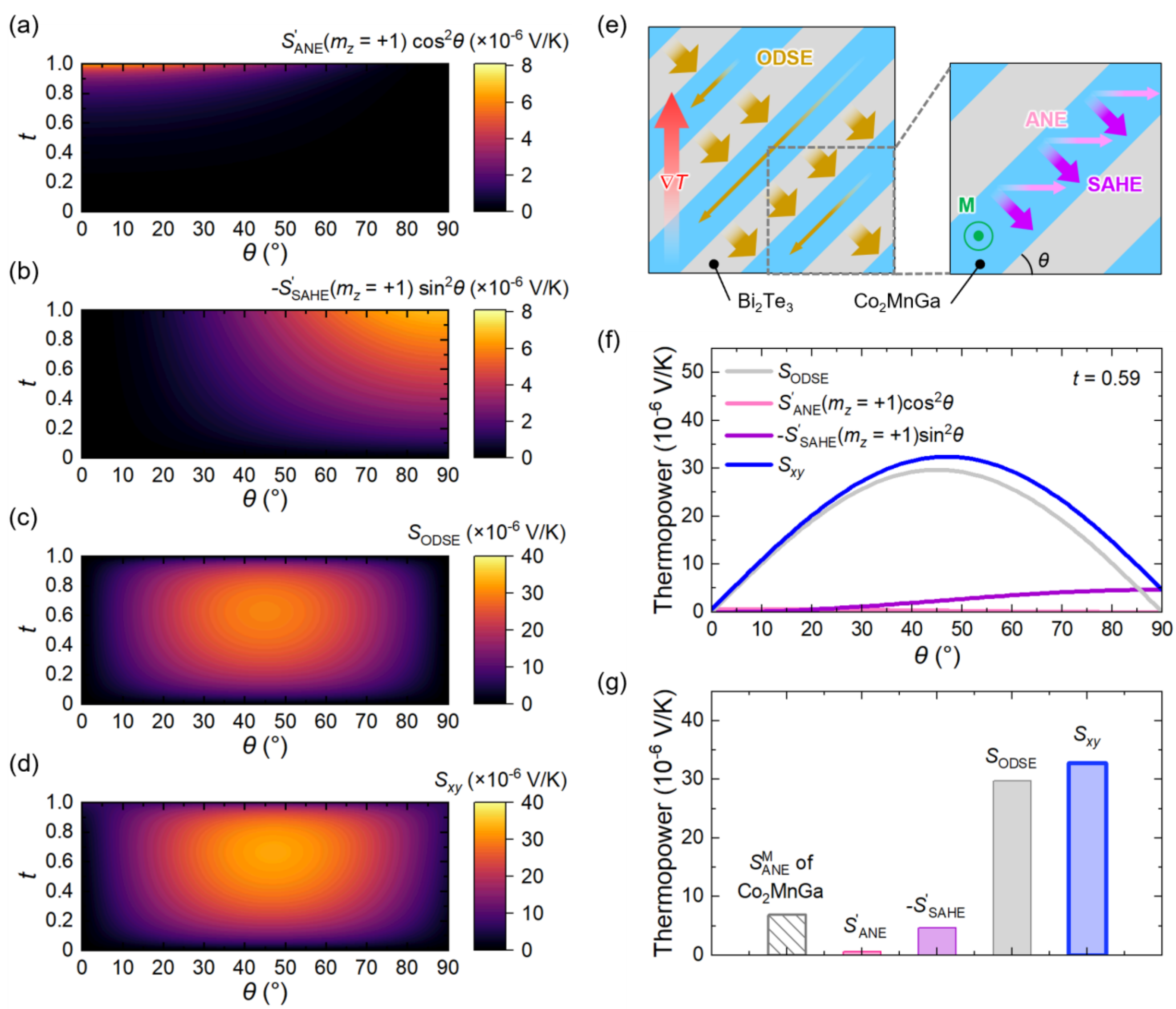

FIG 2. Contour plots of (a) $S'_{\mathrm{ANE}}(m_z = +1)\cos^2\theta$, (b) $-S'_{\mathrm{SAHE}}(m_z = +1)\sin^2\theta$, (c) S_{ODSE}, and (d) S_{xy} for the Co_2MnGa/Bi_2Te_3-based artificially tilted multilayer. (e) A schematic of the hybridization of ODSE, ANE and SAHE (f) The θ dependence of S_{ODSE}, $S'_{\mathrm{ANE}}(m_z = +1)\cos^2\theta$, $-S'_{\mathrm{SAHE}}(m_z = +1)\sin^2\theta$, and S_{xy} at $t = 0.59$. (g) Maximum values of $S'_{\mathrm{ANE}}(m_z = +1)\cos^2\theta$ at $\theta = 0°$, $-S'_{\mathrm{SAHE}}(m_z = +1)\sin^2\theta$ at $\theta = 90°$, S_{ODSE} at $\theta = 45°$, and S_{xy} at $\theta = 47°$ with $S^{\mathrm{M}}_{\mathrm{ANE}}$ of the plain Co_2MnGa.

*Contact author: ANDO.Fuyuki@nims.go.jp

Figure 2(d)-(e) shows the total S_{xy} with m_z = +1 according to Eq. (9) and a schematic of the hybridization of ODSE, ANE and SAHE in the Co_2MnGa/Bi_2Te_3-based artificially tilted multilayer. The absolute value of S_{xy} increases because both $S'_{ANE}(m_z = +1)\cos^2\theta$ and $-S'_{SAHE}(m_z = +1)\sin^2\theta$ are positively superimposed on S_{ODSE} [Fig. 2(d)]. The generation of **E** by ODSE, ANE, and SAHE is described in Fig. 2(e) according to the material hierarchy. The ODSE-induced **E** is strongly localized in the Bi_2Te_3 layers with large S^{TE}. Meanwhile, the ANE- and SAHE-induced **E** appear in the Co_2MnGa layers, which are oriented in the x-direction and perpendicular to the multilayer, respectively.

To visualize the quantitative impact of the hybridization concept, we plot the θ dependence of S_{ODSE}, $S'_{ANE}(m_z = +1)\cos^2\theta$, $-S'_{SAHE}(m_z = +1)\sin^2\theta$, and S_{xy} at t = 0.59 in Fig. 2(f). It is found that $-S'_{SAHE}(m_z = +1)\sin^2\theta$ modifies S_{xy} more than $S'_{ANE}(m_z = +1)\cos^2\theta$, resulting in the shift of optimum θ to a higher angle than 45°. Here, we compare the maximum values of $S'_{ANE}(m_z = +1)\cos^2\theta$ at θ = 0°, $-S'_{SAHE}(m_z = +1)\sin^2\theta$ at θ = 90°, S_{ODSE} at θ = 45°, and S_{xy} at θ = 47° with S^{M}_{ANE} of the plain Co_2MnGa. Although S'_{ANE} and $-S'_{SAHE}$ are solely lower than S^{M}_{ANE} of 6.9 × 10^{-6} V/K due to the reduced volumetric ratio of Co_2MnGa, S_{xy} reaches 32.4 × 10^{-6} V/K owing to the constructive hybridization with S_{ODSE}. Importantly, the optimum θ and t are different between S_{xy} and S_{ODSE}, which respectively maximizes to be 32.7 × 10^{-6} V/K at θ = 47° and t = 0.67 and 29.7 × 10^{-6} V/K at θ = 45° and t = 0.63. According to Appendix, the modification of θ and t also changes ρ_{xx} and κ_{yy} from 2.28 × 10^{-6} Ω·m and 7.95 W/m·K at θ = 45° and t = 0.63 to 2.19 × 10^{-6} Ω·m and 8.78 W/m·K at θ = 47° and t = 0.67. Considering these θ and t dependences of ρ_{xx} and κ_{yy}, we estimate that $z_{xy}T$ based on the maximum S_{xy} is 14% higher than that based on the maximum S_{ODSE} owing to the square-law characteristics [Eq. (1)]. Thus, these results provide two important ideas to employ the strategy of hybrid transverse magneto-thermoelectric conversion: a requirement to rearrange the artificial structure to maximize S_{xy} and a potentially large impact on the transverse thermoelectric performance toward thermoelectric applications.

B. Finite element calculation

Figure 3 (a)–(b) shows the results of the thermoelectric coupling analysis for temperature T and electric potential V distributions in the Co_2MnGa/Bi_2Te_3-based artificially tilted multilayer with θ = 45° and m_z = 0. The application of ∇T in the y-direction [Fig. 3(a)] induces the oblique V gradient [Fig. 3(b)], that is, the generation of **E** for both the x- and y-directions ($E_x = -dV/dx$ and $E_y = -dV/dy$), which respectively imply ODSE and the conventional Seebeck effect.

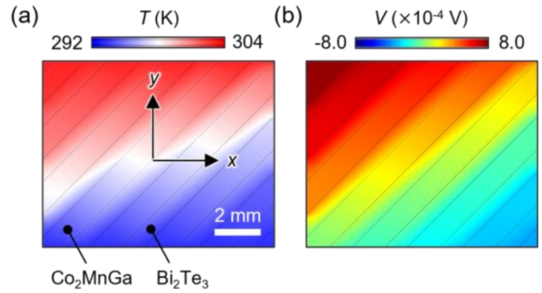

FIG 3. Contour plots of (a) T and (b) V for the Co_2MnGa/Bi_2Te_3-based artificially tilted multilayer with θ = 45° and t = 0.59.

Figure 4(a) shows the m_z dependence of the V distributions under a temperature difference of 10 K for the Co_2MnGa/Bi_2Te_3-based artificially tilted multilayers with θ = 0, 15, 30, 45, 60, 75, and 90°. It is obvious that ODSE and the Seebeck effect predominantly determine the V distribution due to the larger thermopower than magnetization dependent components. ODSE-induced $\mathbf{E}_x$ appears at θ values other than 0° and 90°, which is consistent with the $\sin\theta\cos\theta$ term in Eq. (9). For lower θ values than 45°, the V distributions between m_z = ±1 show negligibly small difference. On the other hand, for higher θ values than 45°, the V distribution is modulated by the sign of m_z. Especially at θ = 90°, the contour plots of V for m_z = ±1 show the upward- and downward-sloping, which means the opposite sign of $\mathbf{E}_x$ depending on the magnetization direction.

To clarify $\mathbf{E}_x$, we plot the x-direction line profile of $V(y = 0)$, which is the average V in the range of –0.1 mm ≤ y ≤ +0.1 mm in Fig. 4(b). For the middle θ values exhibiting ODSE, $V(y = 0)$ shows a step-like behavior due to the inhomogeneous ∇T and thermoelectric property; the Bi_2Te_3 regions exhibit the negative and steep slope due to the negative $\nabla_x T$ (∇T component in the x-direction) and larger S, whereas the Co_2MnGa regions the positive and gentle slope due to the positive $\nabla_x T$ and smaller S. Importantly, only the slope of the Co_2MnGa regions varies depending on the sign of m_z, which suggests the additive contributions by ANE and SAHE and results in the modulation of $\mathbf{E}_x$. Here, the m_z-induced modulation of $\mathbf{E}_x$ becomes larger as θ increases, which is consistent with the larger contribution by $-S'_{SAHE}(m_z = +1)\sin^2\theta$ than that by $S'_{ANE}(m_z = +1)\cos^2\theta$ shown in Fig. 2.

*Contact author: ANDO.Fuyuki@nims.go.jp

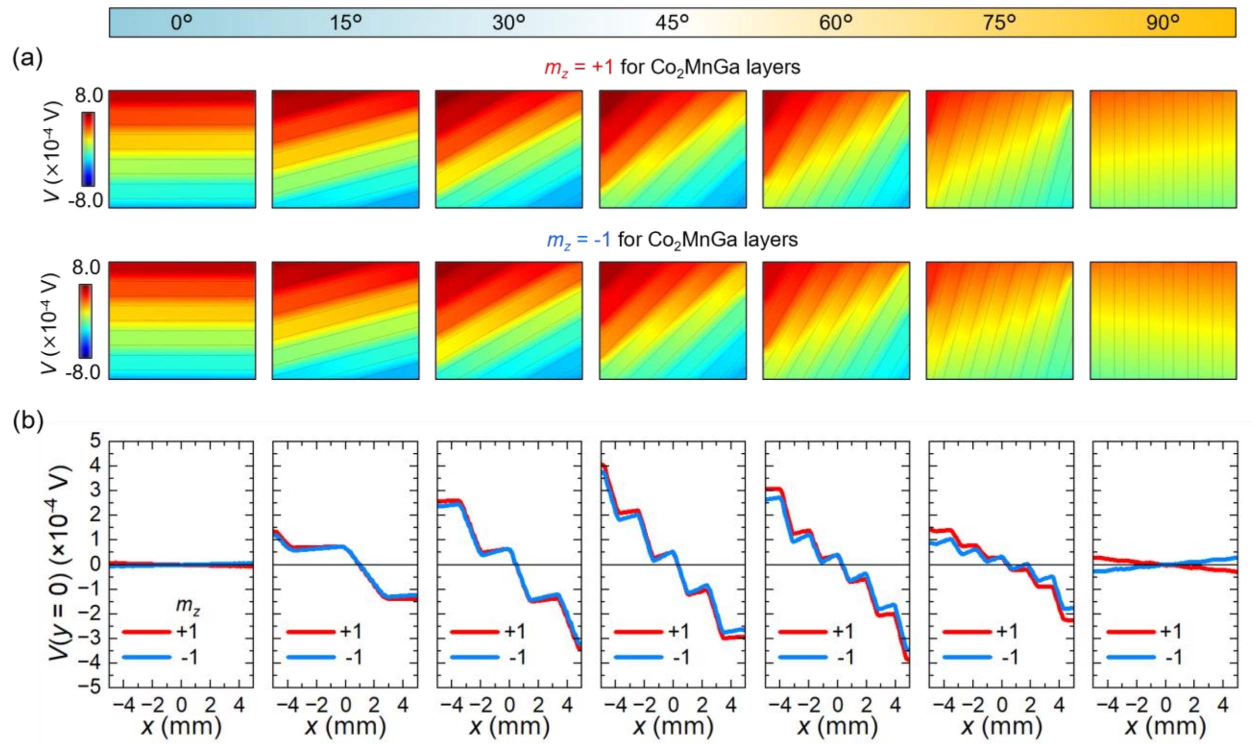

FIG 4. (a) Contour plots of V and (b) line profiles of $V(y = 0)$ in the x-direction for the Co_2MnGa/Bi_2Te_3-based artificially tilted multilayers with various θ values from 0° to 90° and $m_z = \pm 1$.

Let us compare the $S_{xy}(M/H)$ contribution obtained from the tensor calculation and FEM simulation. Figure 5 shows the θ dependence of $S_{xy}(m_z = +1)–S_{xy}(m_z = -1)$, which corresponds to $2[S'_{ANE}(m_z = +1)\cos^2\theta–S'_{SAHE}(m_z = +1)\sin^2\theta]$ in Eqs. (2)-(9) and the difference of $V(y = 0)$ between $x = \pm 5$ mm divided by the applied temperature difference of 10 K for the FEM simulation in Fig. 4(b). These results are quantitatively consistent with each other, showing the increasing trend with increasing θ. Thus, we confirm the appearance and spatial distribution of the transverse thermoelectric effect solved in Eqs. (2)-(9).

IV. DISCUSSION

Finally, we discuss the future perspective to design artificially tilted multilayers using Eqs. (2)-(9) for experiments. As discussed above, the most important message is that, to maximize S_{xy}, one needs to combine magnetic and thermoelectric materials following the inequalities (10)–(11) and rearrange t and θ values from those optimized only for ODSE. As the exploration of magnetic materials having the larger S_{ANE} and $\tan\theta_{AHE}$ than Co_2MnGa progresses, the rearrangement proposed in this work will have a significant impact on the transverse thermoelectric performance. Note that although the combination of Co_2MnGa and n-type Bi_2Te_3 provides the constructive hybridization of ANE and SAHE, in the sense of S_{ODSE} as Eq. (11), one needs to combine materials with the largely different S^M and S^{TE}. Thus, the simultaneous tuning of S, S_{ANE}, and $\tan\theta_{AHE}$ is crucial to constructively utilize all the thermoelectric effects. As demonstrated in Figs. 3 and 4, both the ANE and SAHE contributions occur even in the mm-scale thickness and sample size. Thus, we can adopt typical sintering methods, such as spark plasma sintering, to experimentally create the artificially tilted multilayers for the hybrid transverse magneto-thermoelectric conversion.

On the other hand, there are three possible sources which may cause a deviation of S_{xy} from the calculated one. First, this work neglects the magneto-Seebeck, ordinary Nernst, and Hall effects by the application of **H** to simplify the discussion. However, the stray field due to magnetic layers will induce these **H**-dependent magneto-thermoelectric effects and slightly modulate

*Contact author: ANDO.Fuyuki@nims.go.jp

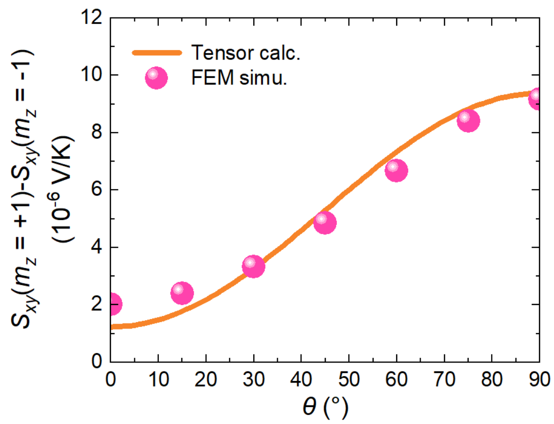

FIG 5. The θ dependence of transverse magneto-thermopower component $S_{xy}(m_z = +1)$–$S_{xy}(m_z = -1)$ obtained from the tensor calculation and FEM simulation.

S_{xy} [46,54]. Second, the thermal boundary condition in the x-direction can influence S_{xy}. When a target material is thermally adiabatic in the **E** direction, S_{xy} includes a parasitic Seebeck contribution by the transverse heat current generation, i.e., the off-diagonal thermal conduction due to an axis-dependent conduction polarity [35,52] and Righi-Leduc effect in magnetic layers [51,55,56]. Third, the interfacial electrical resistance or the formation of interfacial diffusion layers between magnetic and thermoelectric layers can modulate the SAHE contribution because the Seebeck-effect-induced electric field in magnetic layers depends on the interface condition. In fact, while the ANE contribution was clearly measured for Co_2MnGa/Bi_2Te_3- and $Co_2MnGa/Bi_{0.2}Sb_{1.8}Te_3$- based artificially tilted multilayers, the SAHE contribution was hardly observed [47]. Please note that our framework is limited in an ideally high SAHE regime. On the other hand, if one inputs $\tan\theta_{\mathrm{AHE}} = 0$ in Eq. (4), it transforms into no SAHE limit.

V. CONCLUSIONS

We phenomenologically formulated the equations of hybrid transverse magneto-thermopower S_{xy} for artificially tilted multilayers consisting of magnetic and thermoelectric materials for the optimum structural design. It is found that the $S'_{\mathrm{SAHE}}(m_z)\sin^2\theta$ term shows larger values in the wide range of t and θ than the $S'_{\mathrm{ANE}}(m_z)\cos^2\theta$ term due to the constructive contribution by SAHE in addition to ANE. These magnetization-dependent contributions modify the optimum t and θ values to maximize S_{xy}. In case of the Co_2MnGa/Bi_2Te_3-based artificially tilted multilayer, the hybridization of ANE and SAHE is expected to increase $z_{xy}T$ up to 14% owing to the square-law characteristics of S_{xy}. We performed an FEM thermoelectric coupling analysis for the Co_2MnGa/Bi_2Te_3-based artificially tilted multilayer, confirming the appearance of the transverse thermoelectric effects solved by phenomenological formulation. This work will be a guideline to design artificially tilted multilayers with high transverse thermoelectric performance through the hybridization of magneto-thermoelectric phenomena.

ACKNOWLEDGMENTS

The authors thank Y. Yamashita and T. Yagi for valuable discussions. This work was supported by ERATO "Magnetic Thermal Management Materials" (No. JPMJER2201) from JST, Grants-in-Aid for Scientific Research KAKENHI (No. 24K17610) from JSPS, and Resonac Holdings Corporation.

APPENDIX: CALCURATION OF TRANSPORT TENSORS

The electrical resistivity and thermal conductivity tensors (ρ_{ij} and κ_{ij}) are formulated for artificially tilted multilayers based on the Goldsmid's method [41]. In the $x'y'z'$ Cartesian coordinate, the electrical resistivities and thermal conductivities in x'- and y'-directions are analytically calculated as follows:

$$\rho'_{xx} = \frac{1}{t\sigma^{\mathrm{M}} + (1-t)\sigma^{\mathrm{TE}}}, \quad \text{(A1)}$$

$$\rho'_{yy} = \frac{t\sigma^{\mathrm{TE}} + (1-t)\sigma^{\mathrm{M}}}{\sigma^{\mathrm{M}} \cdot \sigma^{\mathrm{TE}}}, \quad \text{(A2)}$$

$$\kappa'_{xx} = t\kappa^{\mathrm{M}} + (1-t)\kappa^{\mathrm{TE}}, \quad \text{(A3)}$$

$$\kappa'_{yy} = \frac{\kappa^{\mathrm{M}} \cdot \kappa^{\mathrm{TE}}}{t\kappa^{\mathrm{TE}} + (1-t)\kappa^{\mathrm{M}}}. \quad \text{(A4)}$$

Following the same coordinate transformation by a rotation matrix as Eq. (8), S_{ij} and ρ_{ij} in the xyz Cartesian coordinate are obtained. The components relevant to this work are shown as

$$\rho_{xx} = \rho'_{xx}\cos^2\theta + \rho'_{yy}\sin^2\theta, \quad \text{(A5)}$$

$$\kappa_{yy} = \kappa'_{xx}\sin^2\theta + \kappa'_{yy}\cos^2\theta. \quad \text{(A6)}$$

*Contact author: ANDO.Fuyuki@nims.go.jp

[1] A. Von Ettingshausen and W. Nernst, Ueber das Auftreten electromotorischer Kräfte in Metallplatten, welche von einem Wärmestrome durchflossen werden und sich im magnetischen Felde befinden, Ann. Phys. **265**, 343 (1886).
[2] M. H. Norwood, Theory of Nernst Generators and Refrigerators, J. Appl. Phys. **34**, 594 (1963).
[3] K. Uchida and J. P. Heremans, Thermoelectrics: From longitudinal to transverse, Joule **6**, 2240 (2022).
[4] H. Adachi, F. Ando, T. Hirai, R. Modak, M. Grayson, and K. Uchida, Fundamentals and Advances in Transverse Thermoelectrics, Appl. Phys. Express **18**, 090101 (2025).
[5] D. Michael. Rowe, *Thermoelectrics Handbook : Macro to Nano* (CRC Press, New York, 2006).
[6] G. Min and D. M. Rowe, Optimisation of thermoelectric module geometry for "waste heat" electric power generation, J. Power Sources **38**, 253 (1992).
[7] F. Ando, H. Tamaki, Y. Matsumura, T. Urata, T. Kawabe, R. Yamamura, Y. Kaneko, R. Funahashi, and T. Kanno, Dual-boost thermoelectric power generation in a GeTe/Mg_3Sb_2-based module, Mater. Today Phys. **36**, 101156 (2023).
[8] T. Kanno, F. Ando, Y. Matsumura, T. Urata, H. Tamaki, and R. Funahashi, Avoiding errors in efficiency measurements of high-performance thermoelectric generator modules: Toward best practices for materials researchers, Mater. Today Phys. **36**, 101171 (2023).
[9] G. E. W. Bauer, E. Saitoh, and B. J. Van Wees, Spin caloritronics, Nat. Mater. **11**, 391 (2012).
[10] S. R. Boona, R. C. Myers, and J. P. Heremans, Spin caloritronics, Energy Environ. Sci. **7**, 885 (2014).
[11] K. Uchida, Transport phenomena in spin caloritronics, Proc. Jpn. Acad. B **97**, 69 (2021).
[12] B. Yan and C. Felser, Topological Materials: Weyl Semimetals, Annu. Rev. Condens. Matter Phys. **8**, 337 (2017).
[13] C. Fu, Y. Sun, and C. Felser, Topological thermoelectrics, APL Mater. **8**, 040913 (2020).
[14] B. A. Bernevig, C. Felser, and H. Beidenkopf, Progress and prospects in magnetic topological materials, Nature **603**, 41 (2022).
[15] T. C. Harman, J. M. Honig, S. Fischler, and A. E. Paladino, The Nernst-Ettingshausen energy conversion figure of merit for Bi and Bi-4% Sb alloys, Solid. State. Electron. **7**, 505 (1964).
[16] W. M. Yim and A. Amith, Bi-Sb alloys for magneto-thermoelectric and thermomagnetic cooling, Solid. State. Electron. **15**, 1141 (1972).
[17] M. Ikhlas, T. Tomita, T. Koretsune, M. T. Suzuki, D. Nishio-Hamane, R. Arita, Y. Otani, and S. Nakatsuji, Large anomalous Nernst effect at room temperature in a chiral antiferromagnet, Nat. Phys. **13**, 1085 (2017).
[18] A. Sakai et al., Giant anomalous Nernst effect and quantum-critical scaling in a ferromagnetic semimetal, Nat. Phys. **14**, 1119 (2018).
[19] H. Reichlova et al., Large anomalous Nernst effect in thin films of the Weyl semimetal Co_2MnGa, Appl. Phys. Lett. **113**, 212405 (2018).
[20] A. Miura, H. Sepehri-Amin, K. Masuda, H. Tsuchiura, Y. Miura, R. Iguchi, Y. Sakuraba, J. Shiomi, K. Hono, and K. Uchida, Observation of anomalous Ettingshausen effect and large transverse thermoelectric conductivity in permanent magnets, Appl. Phys. Lett. **115**, 222403 (2019).
[21] A. Sakai et al., Iron-based binary ferromagnets for transverse thermoelectric conversion, Nature **581**, 53 (2020).
[22] Y. Pan, C. Le, B. He, S. J. Watzman, M. Yao, J. Gooth, J. P. Heremans, Y. Sun, and C. Felser, Giant anomalous Nernst signal in the antiferromagnet $YbMnBi_2$, Nat. Mater. **21**, 203 (2022).
[23] P. Li, P. Qiu, Q. Xu, J. Luo, Y. Xiong, J. Xiao, N. Aryal, Q. Li, L. Chen, and X. Shi, Colossal Nernst power factor in topological semimetal $NbSb_2$, Nat. Commun. **13**, (2022).
[24] F. Ando, T. Hirai, and K. Uchida, Permanent-magnet-based transverse thermoelectric generator with high fill factor driven by anomalous Nernst effect, APL Energy **2**, 016103 (2024).
[25] B. Madavali, F. Ando, T. Hirai, A. Martin-Cid, K. Uchida, and H. Sepehri-Amin, Systematic investigation on transverse thermoelectric conversion of $RE_2(Fe,Co)_{14}B$ (RE = rare-earth) compounds, Sci. Technol. Adv. Mater. **26**, 2520162 (2025).

*Contact author: ANDO.Fuyuki@nims.go.jp

[26] T. C. Chuang, P. L. Su, P. H. Wu, and S. Y. Huang, Enhancement of the anomalous Nernst effect in ferromagnetic thin films, Phys. Rev. B **96**, 174406 (2017).
[27] B. He, C. Şahin, S. R. Boona, B. C. Sales, Y. Pan, C. Felser, M. E. Flatté, and J. P. Heremans, Large magnon-induced anomalous Nernst conductivity in single-crystal MnBi, Joule **5**, 3057 (2021).
[28] R. Gautam, T. Hirai, A. Alasli, H. Nagano, T. Ohkubo, K. Uchida, and H. Sepehri-Amin, Creation of flexible spin-caloritronic material with giant transverse thermoelectric conversion by nanostructure engineering, Nat. Commun. **15**, 2184 (2024).
[29] K. Yamamoto, R. Iguchi, A. Miura, W. Zhou, Y. Sakuraba, Y. Miura, and K. Uchida, Phenomenological analysis of transverse thermoelectric generation and cooling performance in magnetic/thermoelectric hybrid systems, J. Appl. Phys. **129**, 223908 (2021).
[30] W. Zhou, K. Yamamoto, A. Miura, R. Iguchi, Y. Miura, K. Uchida, and Y. Sakuraba, Seebeck-driven transverse thermoelectric generation, Nat. Mater. **20**, 463 (2021).
[31] W. Zhou, T. Sasaki, K. Uchida, and Y. Sakuraba, Direct-Contact Seebeck-Driven Transverse Magneto-Thermoelectric Generation in Magnetic/Thermoelectric Bilayers, Adv. Sci. **11**, 2308543 (2024).
[32] J. Ha, M. Y. Kim, S. J. Park, and H. Jin, Realizing Seebeck-driven transverse thermoelectric generation in bulk composites, Mater. Today Phys. **60**, 101976 (2026).
[33] B. He, Y. Wang, M. Q. Arguilla, N. D. Cultrara, M. R. Scudder, J. E. Goldberger, W. Windl, and J. P. Heremans, The Fermi surface geometrical origin of axis-dependent conduction polarity in layered materials, Nat. Mater. **18**, 568 (2019).
[34] M. R. Scudder, B. He, Y. Wang, A. Rai, D. G. Cahill, W. Windl, J. P. Heremans, and J. E. Goldberger, Highly efficient transverse thermoelectric devices with Re_4Si_7 crystals, Energy Environ. Sci. **14**, 4009 (2021).
[35] M. R. Scudder, K. G. Koster, J. P. Heremans, and J. E. Goldberger, Adiabatic and isothermal configurations for Re_4Si_7 transverse thermoelectric power generators, Appl. Phys. Rev. **9**, 021420 (2022).
[36] Y. Goto, H. Usui, M. Murata, J. E. Goldberger, J. P. Heremans, and C. H. Lee, Band Anisotropy Generates Axis-Dependent Conduction Polarity of Mg_3Sb_2 and Mg_3Bi_2, Chem. Mater. **36**, 2018 (2024).
[37] H. Manako, S. Ohsumi, Y. J. Sato, R. Okazaki, and D. Aoki, Large transverse thermoelectric effect induced by the mixed-dimensionality of Fermi surfaces, Nat. Commun. **15**, 3907 (2024).
[38] C. Zhou, S. Birner, Y. Tang, K. Heinselman, and M. Grayson, Driving Perpendicular Heat Flow: ($p\times n$)-Type Transverse Thermoelectrics for Microscale and Cryogenic Peltier Cooling, Phys. Rev. Lett. **110**, 227701 (2013).
[39] Y. Tang, B. Cui, C. Zhou, and M. Grayson, $p \times n$-Type Transverse Thermoelectrics: A Novel Type of Thermal Management Material, J. Electron. Mater. **44**, 2095 (2015).
[40] C. Reitmaier, F. Walther, and H. Lengfellner, Transverse thermoelectric devices, Appl. Phys. A Mater. Sci. Process. **99**, 717 (2010).
[41] H. J. Goldsmid, Application of the transverse thermoelectric effects, J. Electron. Mater. **40**, 1254 (2011).
[42] T. Kanno, K. Takahashi, A. Sakai, H. Tamaki, H. Kusada, and Y. Yamada, Detection of thermal radiation, sensing of heat flux, and recovery of waste heat by the transverse thermoelectric effect, J. Electron. Mater. **43**, 2072 (2014).
[43] X. Mu, H. Zhou, W. Zhao, D. He, W. Zhu, X. Nie, Z. Sun, and Q. Zhang, High-performance $YbAl_3/Bi_{0.5}Sb_{1.5}Te_3$ artificially tilted multilayer thermoelectric devices via material genome engineering method, J. Power Sources **430**, 193 (2019).
[44] F. Ando, T. Hirai, A. Alasli, H. Sepehri-Amin, Y. Iwasaki, H. Nagano, and K. Uchida, Multifunctional composite magnet realizing record-high transverse thermoelectric generation, Energy Environ. Sci. **18**, 4068 (2025).
[45] M. Murata, F. Ando, T. Hirai, H. Adachi, and K. Uchida, Quantitative measurements of transverse thermoelectric generation and cooling performances in $SmCo_5/Bi_{0.2}Sb_{1.8}Te_3$-based artificially tilted multilayer module, Sci. Technol. Adv. Mater. **26**, 2535955 (2025).
[46] K. Uchida, T. Hirai, F. Ando, and H. Sepehri-Amin, Hybrid Transverse Magneto-Thermoelectric Cooling in Artificially Tilted Multilayers, Adv. Energy Mater. **14**, 2302375 (2024).
[47] T. Hirai, F. Ando, H. Sepehri-Amin, and K. Uchida, Hybridizing anomalous Nernst effect

*Contact author: ANDO.Fuyuki@nims.go.jp

in artificially tilted multilayer based on magnetic topological material, Nat. Commun. **15**, 9643 (2024).
[48] Y. Lee, F. Ando, T. Hirai, R. Modak, H. Sepehri-Amin, and K. Uchida, Zero-Field Hybridization of Anomalous Nernst and Off-diagonal Seebeck Effects in Artificially Tilted Multilayers, Ann. Phys. **537**, e00127 (2025).
[49] P. Tiwari, D. Sahani, A. Chakraborty, K. Das, K. Watanabe, T. Taniguchi, A. Agarwal, and A. Bid, Observation of the Time-Reversal Symmetric Hall Effect in Graphene-WSe_2 Heterostructures at Room Temperature, Nano Lett. **23**, 6792 (2023).
[50] A. W. Smith and A. W. Smith, The Leduc Effect in Some Metals and Alloys, Phys. Rev. **5**, 35 (1915).
[51] F. Ando, Y. Sakuraba, W. Zhou, T. Hirai, and K. Uchida, All electrical detection of thermal Hall angle by on-slab thermocouples, Appl. Phys. Lett. **127**, 222408 (2025).
[52] F. Ando, T. Hirai, H. Adachi, and K. Uchida, Adiabatic transverse thermoelectric conversion enhanced by heat current manipulation in artificially tilted multilayers, Phys. Rev. Appl. **23**, 064061 (2025).
[53] K. Oyanagi et al., Simultaneous achievement of large anomalous Nernst effect and reduced thermal conductivity in sintered polycrystalline topological Heusler ferromagnets, Acta Mater. **296**, 121239 (2025).
[54] M. Murata, T. Hirai, T. Seki, and K. Uchida, Zero-magnetic-field operation of ordinary-Nernst-effect-based transverse thermoelectric module using embedded permanent magnets, Appl. Phys. Lett. **124**, 193901 (2024).
[55] L. Xu, X. Li, L. Ding, T. Chen, A. Sakai, B. Fauqué, S. Nakatsuji, Z. Zhu, and K. Behnia, Anomalous transverse response of Co_2MnGa and universality of the room-temperature $\alpha_{ij}^A/\sigma_{ij}^A$ ratio across topological magnets, Phys. Rev. B **101**, 180404(R) (2020).
[56] T. Imamura, T. Hirai, K. Oyanagi, R. Iguchi, K. Takamori, S. Kobayashi, and K. Uchida, Quantitative noncontact measurement of thermal Hall angle and transverse thermal conductivity by lock-in thermography, Phys. Rev. Appl. **23**, 024018 (2025).

*Contact author: ANDO.Fuyuki@nims.go.jp